

ACCEPTED MAY 18TH 2024

SIMULATION OF MAGNETO-NANO-BIOCONVECTIVE COATING FLOW WITH BLOWING AND MULTIPLE SLIP EFFECTS

O. Anwar Bég^a, Debasis Kumar^b, M.J Uddin^{c}, Md. Abdul Alim^d and T. A. Bég^e*

^a *Professor and Director: Multi-Physical Engineering Sciences Group (MPESG), Mechanical Engineering Department, Corrosion Lab, 3-08, SEE Bldg, Salford University, Manchester, M54WT, UK, Email:*

O.A.Beg@salford.ac.uk

^b *Junior Research Fellow of Autonomous Driving, Institute of Computer Science, University of Tartu, Estonia.*

Email : debasis.kumar@ut.ee

^c *Professor, Mathematics Dept. and Convener: Office of Research, American International University- Bangladesh, Dhaka-1229, Bangladesh. Email : drjashim@aiub.edu*

^d *Department of Mathematics, Bangladesh University of Engineering and Technology (BUET), Dhaka-1000, Bangladesh. Email: maalim@math.buet.ac.bd*

^e *Engineering Mechanics Research, Israfil House, Dickenson Rd., Manchester, M13, UK. Email: tasveerabeg@gmail.com*

**Corresponding author. E-mail address: drjashim@aiub.edu*

Abstract

The phenomenon of bioconvection due to motile microorganism swimming patterns has been found to be a beneficial mechanism in many biological processes and microdevices. Inducing convective transport in self-propelling microbes has been successfully used to enhance mixing, reaction propensity and concentration transport within a range of engineered devices. Doping materials with microorganisms can also be implemented to manipulate magnetohydrodynamic coating processes with smart functional liquids, in which the substrate may be planar, wedge-shaped, curved etc. Inspired by this application, the current article examines theoretically and numerically the external boundary layer Falkner-Skan flow of an electroconductive nanofluid containing gyrotactic micro-organisms on a two-dimensional wedge with Stefan blowing and different slip effects at the wedge boundary. The physico-mathematical model is formulated using a system of partial differential equations and appropriate boundary conditions which are then transformed to a system of ordinary differential equations with appropriate similarity variables. The non-dimensional boundary value problem is solved numerically with the aid of the Mathematica software solver package named “NDSolve”. The impacts of the Stefan blowing, velocity, thermal, nanoparticle concentration and microorganism slips, magnetic number, Lewis number, bioconvection Lewis number, the Falkner-Skan wedge parameter, bioconvection Péclet number, thermophoresis and Brownian motion on key transport characteristics i.e. dimensionless velocity, temperature, nanoparticle concentration (volume fraction), microorganism concentration, skin friction coefficient, local heat transfer rate (local Nusselt number), local mass transfer rate (local Sherwood number) and the microorganism local density number gradient are computed and visualized graphically. Numerical solutions are validated with previous literature. The outcomes reported in this paper are relevant to the synthesis of functional bio-nanopolymers.

Keywords: *Stefan blowing; Bio-nanofluid; Slips Effects; Wedge Flow; NDSolve; Materials processing.*

Nomenclature

a	velocity slip parameter (–)
a_0	arbitrary constant (s^{-1})
b	thermal slip parameter (–)
\bar{b}	chemotaxis constant (m)
B	variable magnetic field ($(kg) A^{-1} s^{-2}$)
B_0	constant magnetic field ($(kg) A^{-1} s^{-2}$)
C	nanoparticle volume fraction (–)
C_w	wall nanoparticle volume fraction (–)
C_∞	ambient nanoparticle volume fraction (–)
d	mass slip parameter (–)
D_1	variable thermal slip factor (m)
$(D_1)_0$	constant thermal slip factor (m)
D_B	Brownian diffusion coefficient ($m^2 s^{-1}$)
D_n	diffusivity of microorganisms ($m^2 s^{-1}$)
D_T	thermophoretic diffusion coefficient ($m^2 s^{-1}$)
e	microorganism slip parameter (–)
E_1	variable concentration slip factor (m)
$(E_1)_0$	constant concentration slip factor (m)
$f(\eta)$	dimensionless stream function (–)
F_1	variable microorganism slip factor (m)
$(F_1)_0$	constant microorganism slip factor (m)
k	thermal conductivity ($Wm^{-1} K^{-1}$)
K	arbitrary constant (–)
Lb	bioconvection Lewis number (–)
Le	Lewis number (–)
m	wedge parameter (–)
M	magnetic number (–)
N	volume fraction of motile microorganisms (–)
N_1	variable velocity slip factor ($s m^{-1}$)
$(N_1)_0$	constant velocity slip factor ($s m^{-1}$)
Nb	Brownian motion parameter (–)
Nn_x	local density number of the motile microorganisms (–)
Nt	thermophoresis parameter (–)
Nu_x	local Nusselt number (–)

N_w	wall microorganism (–)
N_∞	ambient microorganism (–)
Pe	bioconvection Péclet number (–)
Pr	Prandtl number (–)
S	Stefan blowing parameter (–)
Sh_x	local Sherwood number (–)
T	nanofluid temperature (K)
T_w	wall temperature (K)
T_∞	ambient temperature (K)
u, v	velocity components along the x - and y - axes ($m s^{-1}$)
\tilde{v}	microorganism swimming velocity ($m s^{-1}$)
u_e	ambient velocity ($m s^{-1}$)
W_c	maximum cell swimming speed ($m s^{-1}$)
x, y	Cartesian coordinates (x -axis is aligned along and y -axis is normal to the wedge) (m)

Greek symbols

α	effective thermal diffusivity ($m^2 s^{-1}$)
η	similarity variable (–)
$\theta(\eta)$	dimensionless temperature (–)
μ	dynamic viscosity ($(kg) m^{-1} s^{-1}$)
ν	kinematic viscosity of the fluid ($m^2 s^{-1}$)
ρ	the density of the base fluid ($(kg) m^{-3}$)
σ	electric conductivity ($(kg)^{-1} m^{-3} s^3 A^2$)
$\chi(\eta)$	the rescaled density of motile microorganisms (–)
τ	ratio between the effective heat capacity of the nanoparticle material and heat capacity of the fluid (–)
$\phi(\eta)$	rescaled nanoparticle volume fraction (–)
ψ	stream function (–)

Subscripts/superscripts

w	condition at the wall
-----	-----------------------

1. Introduction

Liquid thermal properties are crucial for heating and cooling applications in several industrial processes. Because of their lower thermal conductivity, conventional heat transfer fluids are unsuitable for applications requiring extremely high cooling. Applied mathematicians, engineers, and scientists have attempted to use solids suspended in particulate form in carrier fluids to enhance the conventional heat transfer fluids' intrinsically low thermal conductivity

[1]. The deployment of solid particles from the millimeter to the micrometer ranges for achieving improved thermophysical properties has unsuccessful due to several issues, including particle sedimentation, excessive pressure drops, corrosion of components of machines, particle clogging (agglomeration), low thermal conductivity, etc. This has necessitated further scaling down of particle dimensions to mitigate the drawbacks encountered with micrometer/millimeter scale suspensions in order to achieve the desired elevation in thermal properties and heat transfer performance. These efforts have resulted in a revolutionary concept known as *nanofluids*, which utilizes engineering at the nanoscale, i.e., *nanotechnology* via a range of chemical and physical methods to fabricate particles having diameter 10^{-9} meter. Nanofluids are, therefore, concocted on the atomic scales with superior thermo-physical characteristics than their bulk counterparts. Choi [2] and Lee [3] demonstrated that nanofluids, i.e., colloidal liquids containing nanoparticles, successfully achieve thermal enhancement and superior performance in many applications. Considering published literature, nanoparticles can be manufactured from a wide spectrum of appropriate materials, namely metals (**Copper, Silver, Gold**), semiconductors (**SiC**), oxide ceramics, nitride ceramics, and carbide ceramics, carbon nanotubes etc. Nanofluids comprise both an original carrier fluid with nanoparticles. They are designed to attain the best possible thermal properties with the least amount of nanoparticle volume fraction by even spreading and stable suspension of nanoparticles in carrier fluids (Murshed *et al.* [4] and Kakac *et al.* [5]). Nanofluids are capable of boosting key physical properties like thermal/mass diffusivity and viscosity which are considerably better than the properties of original base fluids like water or oil (Kaufui and Omar [6]). Nanofluids have many applications, such as electronic device cooling, vehicle cooling, transformer cooling, computer cooling, electronics cooling, fuels, coatings, sterilization of biomedica, detergency, etc. Ultra-high-performance heating and cooling, which is achievable with nanofluids, is useful for many industrial technologies, including automobile radiators, aerospace propulsion ducts, semiconductor manufacture, nuclear reactor thermal control, solar power collectors, etc.

Nanofluids, in particular, provide an excellent methodology for the production of next-generation functional (smart) coatings wherein wall heat transfer and momentum transfer characteristics can be very carefully manipulated to achieve a range of high-quality, durable designs for deployment in many complex sectors. Coating processing is often conducted in manufacturing on simple substrate geometries, including flat, continuously moving surfaces, inclined planes, and wedges. Such applications feature boundary layer flows, which are

generally laminar and incompressible owing to the high densities of coating materials and low speeds of production. Many different materials are manufactured in this fashion, including polymers, adhesives, foodstuffs, and, more recently, nano-liquid coatings. Historically, the first comprehensive examination of two-dimensional wedge boundary layer external flow was presented by Falkner and Skan [7], who considered the steady incompressible Newtonian flow impinging on a two-dimensional wedge geometry with an apex angle of $\pi\beta$ accompanied by an inviscid external flow and an external pressure gradient. They derived a series of solutions for special cases of the apex angle and pressure gradient parameter, including forward stagnation flow, Blasius flow, Hiemenz stagnation flow, flow with an adverse pressure gradient, and flow from a vertical surface. This category of flows has come to be known as *Falkner-Skan wedge flow*. Many researchers have subsequently extended the Falkner-Skan study to consider other physical effects, including heat transfer, mass transfer, electromagnetic body forces, non-Newtonian behavior, and, more recently, nanofluids, which also arise in industrial coating operations. These studies have utilized various numerical methods due to the inherent nonlinearity of Falkner-Skan wedge flows. Gaffar *et al.* [8] deployed the Keller box finite difference method to compute the mixed convective non-Newtonian flow from a wedge with convective wall heating, noting that magnetic field, rheological parameter, and wedge parameter have a strong influence on skin friction and Nusselt number. Bég *et al.* [9] used HAM to compute the micropolar convective flow from a wedge with viscous heating and heat sink effects. Zueco and Bég [10] implemented a PSPICE-based electrothermal network simulation method (NSM) to calculate thermal radiative flux and magnetic field effects of electroconductive gas flow from a wedge in a non-Darcy porous medium. Zohra *et al.* [11] used a Chebyshev collocation method to analyze the flow of a nanofluid doped with microorganisms from a wedge with a transverse magnetic field and aligned electrical field effects.

A natural propulsion mechanism encountered in certain microorganisms is bioconvection. When a microorganism is denser and heavier than water, it may nevertheless swim in a certain direction and upward. When the top layer is very thick, microorganisms descend, resulting in bioconvection patterns. Certain oxytactic bacteria, like *Bacillus subtilis*, are propelled by the oxygen they consume, i.e., they are oxy-tactic. Through surface diffusion, the oxygen is replenished (Lee and Kim [12]). Engineers have explored the combination of nanoparticles with specific microorganisms in order to control heat and mass transfer rates in

various applications, including coatings, fuel cells, and bioreactors. The resulting regime is known as *nanofluid bioconvection and the fluids can be termed bio-nanofluids*. Shaw *et al.* [13] examined MHD bioconvective flow in a porous media by studying nanofluids doped with gyrotactic microorganisms. Zaimi *et al.* [14] examined the stagnation-point flow of a nanofluid toward a sheet that contained both nanoparticles and microorganisms. Xu and Pop examined boundary layer flow doped with nanoparticles and gyrotactic microorganisms in a horizontal channel using mixed convection flow [15]. Raees *et al.* [16] analyzed mixed convection of gyrotactic microorganisms and nanoparticles in a gravity-driven nano-liquid. Engineers have further explored the simultaneous deployment of magnetic fields in nanofluid bioconvection or “bio-nanofluid” systems. This is known as *magnetohydrodynamic nanofluid bioconvection* and requires simultaneous consideration of viscous hydromagnetics, nanoscale transport and bioconvective transport. It has many potential applications in smart coating systems [17-21], and microorganisms can be *gyrotactic (torque-responsive)*, *photo-tactic (light-responsive)*, *magneto-tactic (magnetic field responsive)*, *chemo-tactic (chemically responsive)*, etc. Magnetic field effects on nanofluid gyrotactic bioconvection from a stretching surface were investigated by Akbar and Khan [22]. Mutuku and Makinde [23] computed the effect of wall suction/injection on hydromagnetic bioconvection nanofluid flow from a permeable vertical wall. Xu [24] considered the influence of an outer power-law stream on nanofluid bioconvection boundary layer transport from a vertical plane with Lie group algebra. Amirson *et al.* [25] analyzed the impact of variable transport properties on a bio-nanofluid's three-dimensional stagnation point flow. Latiff *et al.* [26] studied the swirling flow from a solid rotating disk. Babu and Sandeep [27] investigated the influence of radiation on the magento-bio-convective flow past an extendable sheet. Makinde and Animasaun [28] computed the Brownian motion and thermophoresis effects on MHD bioconvection nanofluid flow external to the upper horizontal surface of a parabolic body with quartic chemical reaction and nonlinear thermal radiation. Uddin *et al.* [29] used a Chebyshev collocation method to compute the effects of thermal and hydrodynamic slip on the wedge flow of a magnetic nanofluid doped with microorganisms. Uddin *et al.* [30] investigated the bioconvection nanofluid slip flow over a wavy (sinusoidal) boundary to simulate hybrid biofuel cells.

Species transfer or mass transfer is common in materials processing operations. It may be controlled via wall perforations in a coating substrate or other external means. *Stefan blowing* is a unique blowing phenomenon that may also be produced by mass transfer. (Nellis and

Klein [31]). The blowing effect generates an exacerbated fluid motion and produces behavior that deviates from conventional flows (Lienhard and Lienhard [32]). There are several distinctions between blowing owing to mass injection/suction at a boundary and the Stefan blowing effect. Mass blowing has an impact on the flow field; there is a dynamic interplay between momentum fields and concentration (Fang [33]). Fang and Jing [34] investigated Stefan blowing effects by species transfer on thermo-solutal convection from a stretching plate. Latiff *et al.* [35] scrutinized the effect of Stefan blowing on the flow of bio-nanofluid from an impervious rotating disk. Uddin *et al.* [36] studied swirling thermo-solutal bio-nanofluid convection from a rotating cone to an anisotropic porous medium with Stefan blowing, Navier slip effects, and radiation. Amirsom *et al.* [37] examined Stefan blowing and phase change heat transfer effects of electromagneto-convective flow of bio-nanofluid. Basir *et al.* [38] analyzed the effect of Stefan blowing and leading-edge accretion/ ablation on bioconvection nanofluid flow. For gyrotactic microorganisms, the effects of Stefan blowing on a nanofluid's MHD bioconvection flow were examined by Giri *et al.* [39] with active and passive nanoparticle flux. Zohra *et al.* [40] evaluated numerically the effect of Stefan blowing and anisotropic slip on magneto-bioconvection nanofluid past a rotating cone. Amirsom *et al.* [41] investigated non-Newtonian MHD bionanoconvective flow over an axisymmetric needle with Stefan blowing effects.

In materials processing operations, slip effects are known to arise at boundaries [42, 43]. This has also been identified in nanomaterial coating flows [44, 45]. Wall slip can significantly modify boundary layer characteristics, including surface heat transfer and skin friction. Nanofluid slip flow MHD effects for coating applications was examined by Uddin *et al.* [46]. In another paper, Uddin *et al.* [47] examined g-jitter oscillation effects on mixed convective slip flow with variable viscosity in a Darcian porous media. Magneto-convective slip flow from a porous sheet was investigated by Uddin *et al.* [48]. Uddin *et al.* [49] evaluated the slip effects on the flow field past a sheet. Temperature jump condition effects on flow from a porous cylinder were investigated by Mishra and Singh [50]. More research on the slip effects using the Navier linear slip model for the flow of power-law liquids from smooth spherical particles was published by Kishore and Ramteke [51]. Shateyi and Mabood [52] investigated MHD mixed convection slip flow near a stagnation point on a nonlinearly vertical stretched sheet in the presence of viscous dissipation. Khan *et al.* [53] analyzed unsteady MHD flow with slip influence of nanofluids. Basir *et al.* [54] computed the impact of Schmidt and Péclet numbers on the slip flow of nanofluids from a stretched cylinder.

Rosca *et al.* 0 enumerated the velocity slip using Buongiorno's mathematical model in nanofluid transport from a porous sheet. All these studies confirmed the substantial impact of wall slip on nanofluids' heat, momentum, and mass transfer characteristics.

In the present article, a mathematical model is developed to study the collective effects of the external magnetic field, Stefan blowing, and multiple boundary slip effects in nanofluid gyrotactic bioconvection from a wedge configuration as a model of nano-bioconvective smart coating processing. The transformed, non-dimensional coupled boundary layer equations for momentum, energy, nanoparticle species diffusion, and microorganism species are solved under carefully prescribed boundary conditions with the NDSolve routine in Mathematica, modified for a finite element technique. Extensive visualization of the influence of key control parameters on boundary layer characteristics is included. Verification of NDSolve solutions via benchmarking with earlier simpler studies from the literature is included. The novelties of the current study are the simultaneous consideration of *4 different wall slip effects, Stefan blowing, and magnetic field* on 2-D Falkner-Skan wedge coating flow dynamics. These have not been reported so far anywhere in the scientific or engineering literature and constitute an important addition to the existing understanding of smart bio-nanocoating fluid dynamics simulation.

2. Nano-bio-boundary layer model for MHD wedge transport

The steady 2-dimensional incompressible gyrotactic bioconvective Falkner-Skan boundary layer flow of electroconductive nanofluid with water as a carrier (base) fluid external to a wedge is investigated. The flow diagram and system of coordinate is presented in **Fig. 1**. A variable magnetic field \vec{B} is applied orthogonal to the wedge face. Electrical polarization, magnetic induction, and Hall current effects are neglected. Viscous dissipation, thermal dispersion, and thermal stratification are also neglected. Buongiorno's two-component nanoscale model is adopted. It is considered that the suspension of nanoparticles is stable. Wedge surface temperature, nanoparticle volume fraction, and density of motile microorganisms are denoted as T_w , C_w , and N_w , although the ambient values are imposed as T_∞ , C_∞ , and N_∞ , respectively.

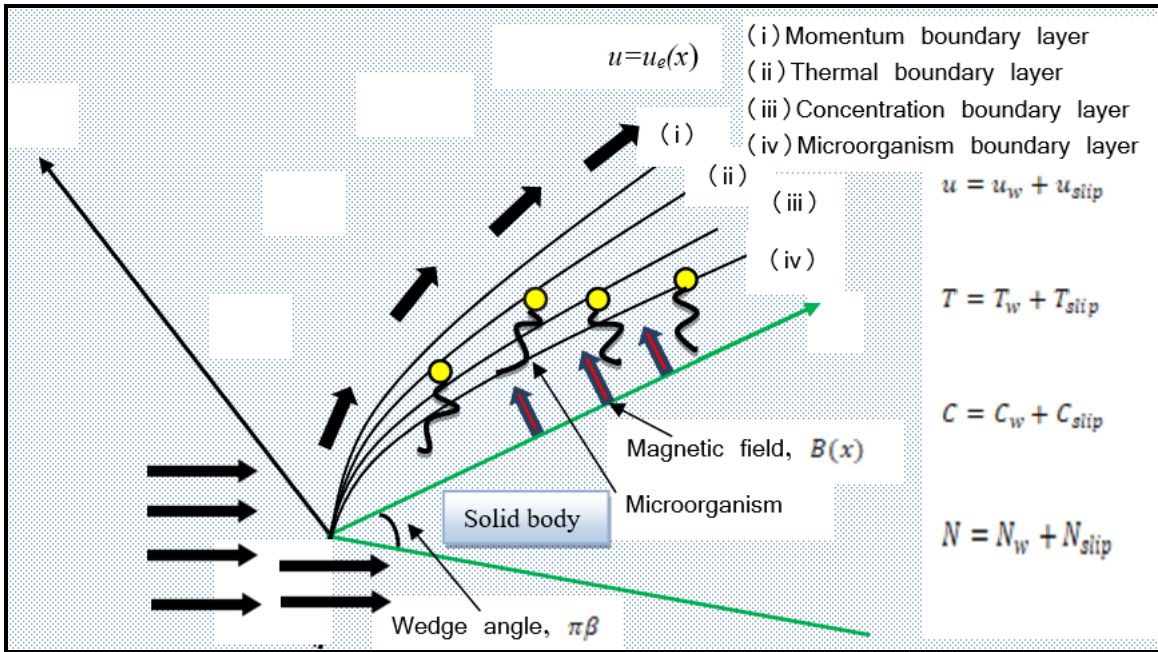


Fig.1: Physical model for hydromagnetic forced bio-nanoconvective wedge coating flow

The governing equations for two-dimensional incompressible laminar flow emerge after amalgamating the models in refs [11], [13], [22] and [23] as:

as:

$$\frac{\partial u}{\partial x} + \frac{\partial v}{\partial y} = 0, \quad (1)$$

$$u \frac{\partial u}{\partial x} + v \frac{\partial u}{\partial y} = K^2 u_e \frac{du_e}{dx} + v \frac{\partial^2 u}{\partial y^2} - (u - Ku_e) \frac{\sigma B^2(x)}{\rho}, \quad (2)$$

$$u \frac{\partial T}{\partial x} + v \frac{\partial T}{\partial y} = \alpha \frac{\partial^2 T}{\partial y^2} + \tau \left[D_B \frac{\partial C}{\partial y} \frac{\partial T}{\partial y} + \left(\frac{D_T}{T_\infty} \right) \left(\frac{\partial T}{\partial y} \right)^2 \right], \quad (3)$$

$$u \frac{\partial C}{\partial x} + v \frac{\partial C}{\partial y} = D_B \frac{\partial^2 C}{\partial y^2} + \left(\frac{D_T}{T_\infty} \right) \frac{\partial^2 T}{\partial y^2}, \quad (4)$$

$$u \frac{\partial N}{\partial x} + v \frac{\partial N}{\partial y} + \frac{\partial}{\partial y} (N\tilde{v}) = D_n \frac{\partial^2 N}{\partial y^2}. \quad (5)$$

Subject to the boundary conditions:

$$u = N_1(x) v \frac{\partial u}{\partial y}, \quad v = -\frac{D_B}{1-C_w} \frac{\partial C}{\partial y}, \quad T = T_w + D_1(x) \frac{\partial T}{\partial y}, \quad (1)$$

$$C = C_w + E_1(x) \frac{\partial C}{\partial y}, \quad \text{and} \quad N = N_w + F_1(x) \frac{\partial N}{\partial y} \quad \text{at} \quad y = 0.$$

$$u = Ku_e(x) = Ka_0 x^m, \quad T = T_\infty, \quad C = C_\infty, \quad N = N_\infty = 0 \quad \text{as} \quad y \rightarrow \infty. \quad (7)$$

Here far field velocity, temperature, nanoparticle volume fraction, microorganism density numbers are denoted respectively by $u_\infty, T_\infty, C_\infty, N_\infty$. N_1, D_1, E_1 , and F_1 stands for velocity, thermal slip, nanoparticle mass, and microorganism slip factor, respectively, \tilde{v} denotes the microorganism swimming velocity, and K, α_0 , and m are constants. Based on Lie group algebra, the following similarity variables are invoked:

$$\begin{aligned} \psi &= \sqrt{u_\infty(x)vx} f(\eta), \quad \eta = \sqrt{\frac{u_\infty(x)}{vx}} y, \quad \theta(\eta) = \frac{T-T_\infty}{\Delta T}, \quad \phi(\eta) = \frac{C-C_\infty}{\Delta C}, \quad \chi(\eta) = \frac{N-N_\infty}{\Delta N}, \\ u &= u_\infty(x) f'(\eta), \quad v = -\frac{m+1}{2} \sqrt{\frac{u_\infty(x)v}{x}} \left[f(\eta) + \frac{m-1}{m+1} \eta f'(\eta) \right], \quad \tilde{v} = \left(\frac{\tilde{v}W_c}{\Delta C} \right) \frac{\partial C}{\partial y}, \\ \Delta T &= T_w - T_\infty, \Delta C = C_w - C_\infty, \Delta N = N_w - N_\infty. \end{aligned} \quad (8)$$

The stream function ψ is defined by $u = \frac{\partial \psi}{\partial y}$ and $v = -\frac{\partial \psi}{\partial x}$. Introducing Eqn. (12) into (7)-(11), the following ordinary differential equations are obtained.

$$f'''' + mK^2 - mf'^2 + \left(\frac{m+1}{2}\right)ff'' - M(f' - K) = 0, \quad (2)$$

$$\theta'' + Pr\left(\frac{m+1}{2}\right)f\theta' + Nb\phi'\theta' + Nt\theta'^2 = 0, \quad (0)$$

$$\phi'' + \left(\frac{m+1}{2}\right)LePrf\phi' + \frac{Nt}{Nb}\theta'' = 0, \quad (3)$$

$$\chi'' + \left(\frac{m+1}{2}\right)Lbf\chi' - Pe[\phi'\chi' + \chi\phi''] = 0. \quad (2)$$

The dimensionless boundary conditions take the form:

$$\begin{aligned} f(0) &= \frac{2S}{(m+1)PrLe} \phi'(0), \quad f'(0) = a f''(0), \quad \theta(0) = 1 + b\theta'(0), \\ \phi(0) &= 1 + d\phi'(0), \quad \chi(0) = 1 + e\chi'(0), \quad f'(\infty) = K, \\ \theta(\infty) &= \phi(\infty) = \chi(\infty) = 0. \end{aligned} \quad (4)$$

The prime stands for differentiation with respect to η . Also, $a = (N_1)_0 \sqrt{va_0}$,

$$\begin{aligned} (N_1)_0 &= N_1(x)x^{\frac{m-1}{2}}, \quad b = (D_1)_0 \sqrt{\frac{a_0}{v}}, \quad (D_1)_0 = D_1(x)x^{\frac{m-1}{2}}, \quad d = (E_1)_0 \sqrt{\frac{a_0}{v}}, \\ (E_1)_0 &= E_1(x)x^{\frac{m-1}{2}}, \quad e = (F_1)_0 \sqrt{\frac{a_0}{v}}, \quad \text{and } (F_1)_0 = F_1(x)x^{\frac{m-1}{2}}. \end{aligned} \quad (5)$$

The dimensionless parameters featured in Eqns. (9)-(13) have the following definitions:

Magnetic number $M = \frac{\sigma B_0^2}{\rho \alpha_n}$ where $B_0(x) = B(x)x^{\frac{1-m}{2}}$, Prandtl number $Pr = \frac{\nu}{\alpha}$, Brownian

motion parameter $Nb = \frac{\tau D_B \Delta C}{\alpha}$, Thermophoresis parameter $Nt = \frac{\tau D_T \Delta T}{T_\infty \alpha}$, Bioconvection Lewis number $Lb = \frac{\nu}{D_n}$, Lewis number $Le = \frac{\alpha}{D_R}$, and bioconvection Péclet number $Pe = \frac{\bar{v} W_c}{D_n}$. Also, $S = (C_w - C_\infty) / (1 - C_w)$ is the Stefan blowing parameter in the wall boundary condition (13).

The main physical quantities to be computed at the wedge surface are the shear stress C_{fx} , the heat transfer gradient, Nu_x , nanoparticle volume fraction gradient Sh_x , and the density motile microorganisms gradient Nn_x . These are defined as:

$$C_{fx} = \frac{\nu}{u_\infty^2(x)} \left(\frac{\partial u}{\partial y} \right)_{y=0} = \left(\sqrt{\frac{\nu}{xu_\infty(x)}} f''(\eta) \right)_{y=0}, \quad (15)$$

$$Nu_x = -\frac{x}{\Delta T} \left(\frac{\partial T}{\partial y} \right)_{y=0} = -\left(\sqrt{\frac{xu_\infty(x)}{\nu}} \theta'(\eta) \right)_{y=0}, \quad (16)$$

$$Sh_x = -\frac{x}{\Delta C} \left(\frac{\partial C}{\partial y} \right)_{y=0} = -\left(\sqrt{\frac{xu_\infty(x)}{\nu}} \phi'(\eta) \right)_{y=0}, \quad (17)$$

$$Nn_x = -\frac{x}{\Delta N} \left(\frac{\partial N}{\partial y} \right)_{y=0} = -\left(\sqrt{\frac{xu_\infty(x)}{\nu}} \chi'(\eta) \right)_{y=0}. \quad (18)$$

By substituting the similarity variables into (16)-(18), the required dimensionless expressions for the wall gradients are:

$$C_{fx} Re_x^{\frac{1}{2}} = f''(0), \quad Nu_x Re_x^{-\frac{1}{2}} = -\theta'(0), \quad (19)$$

$$Sh_x Re_x^{-\frac{1}{2}} = -\phi'(0), \quad Nn_x Re_x^{-\frac{1}{2}} = -\chi'(0),$$

where, $Re_x = \frac{xu_\infty(x)}{\nu}$ is the Reynolds number.

3. Numerical Solution and Validation

The transformed equations (9)-(13) has been simulated numerically with the built-in command NDSolve in Mathematica. It has been used by many researchers, including Fang and Jing [34]. However, in the present study, the original finite difference algorithm is modified in Mathematica 11, with a finite element method. The package “Needs[“NDSolve`FEM`”]” has been downloaded and added the option as

NDSolve[....., Method \rightarrow {"FiniteElement"}] to accomplish the finite element method. The convergence characteristics are excellent (up to seven orders of local accuracy), and it improves on the original NDSolve routine correctness of the simulation with the option "Evaluate[Abs[f'[a - 1] - f'[a]]/.solution], a}], {a, 1, 30, 1}]]. This enables optimized accuracy with the free stream boundary condition (at infinity). To validate the NDSolve finite element modified algorithm, the solutions were associated with the existing analytical solutions of Fang and Jing [34] when *magnetic field, nanofluid, bioconvection, and slip characteristics are negated*, i.e., $M = Nt = Nb = Pe = K = Lb = b = d = e = 0$. Also, $f'(0) = a = m = 1, Pr = 5$ are arranged with various sets of data, i.e., $Le = 0.2, 0.4, 1$, and $2, S = 4, 8, 20$, and 40 to adjust the values of the solutions to conform exactly with $Pr = 5, \gamma = 4$, and $Sc = 1, 2, 5$, and 10 in [34]. Since bioconvection is not considered in [34], but mass transfer is, only the fourth differential equation with corresponding boundary conditions is discounted in our model to replicate the case benchmarked exactly. **Table 1** documents the comparison of solutions. Excellent agreement has been attained with the published results of Fang and Jing [34] for wall nanoparticle mass transfer rate and heat transfer rate, confirming the accuracy of the ND Solve finite element code adopted in the present work. The infinity boundary condition was prescribed as $\eta \rightarrow 25$.

Table 1: Comparison of present study with Fang and Jing [34]

Fang and Jing [34] $Pr = 5,$ $\gamma = 4.$	Present $Pr = 5$ (numerical)	Fang and Jing [34] $-\phi'(0)$	Present study $-\phi'(0)$	Fang and Jing [34] $-\theta'(0)$	Present study $-\theta'(0)$
$Sc = 1$	$Le = 0.2, S = 4$	0.194923	0.194923	0.0915398	0.0915398
$Sc = 2$	$Le = 0.4, S = 8$	0.192341	0.192341	0.0972581	0.097258
$Sc = 5$	$Le = 1, S = 20$	0.167467	0.167467	0.167467	0.167467
$Sc = 10$	$Le = 2, S = 40$	0.142111	0.142111	0.271687	0.271687

4. Results and discussions

Graphical plots for dimensionless velocity, temperature, nanoparticle concentration, and gyrotactic microorganism number density for the effects of various slip and blowing parameters are visualized in **Figs. 2-10**. The default data utilized is $a = b = d = e = M = m = Pe = K = 1, Pr = 6.8, Nb = Nt = 0.1, Le = 2,$ and $Lb = 2$ which represents bio-nano materials coating processing scenarios. In the ensuing discussion, we consider the effects of different physical parameters on all the main transport characteristics.

4.1 Impacts of blowing

Fig. 2(a) illustrates the impact of the Stefan blowing on the velocity. The velocity profiles for *no-slip* boundary conditions are decreased with a positive value of the blowing parameter but increased with a negative value of the Stefan blowing parameter. Positive Stefan blowing therefore increases momentum boundary layer thickness, whereas negative blowing induces the opposite effect. Stefan blowing has little influence when the slip condition is added to the velocity field, whether weak or strong blowing occurs to the wall. Clearly, the combination of slip and Stefan blowing has some interesting effects on the momentum boundary layer, which will modify the coating thickness and homogeneity.

Variations of temperature with blowing parameter is shown in Fig. 2. It is found that temperature is boosted with a positive increment in the Stefan blowing parameter, but the reverse is observed with a negative value of Stefan blowing. Thermal boundary layer thickness is therefore increased with positive Stefan blowing. For both cases, temperature profiles show significant change with Stefan blowing, although the effect is much more prominent in the no-slip case. When $\eta = 0$ was used, the dimensionless temperature profile values were close to 0.4 for the slip boundary conditions and close to one for the no-slip boundary conditions.

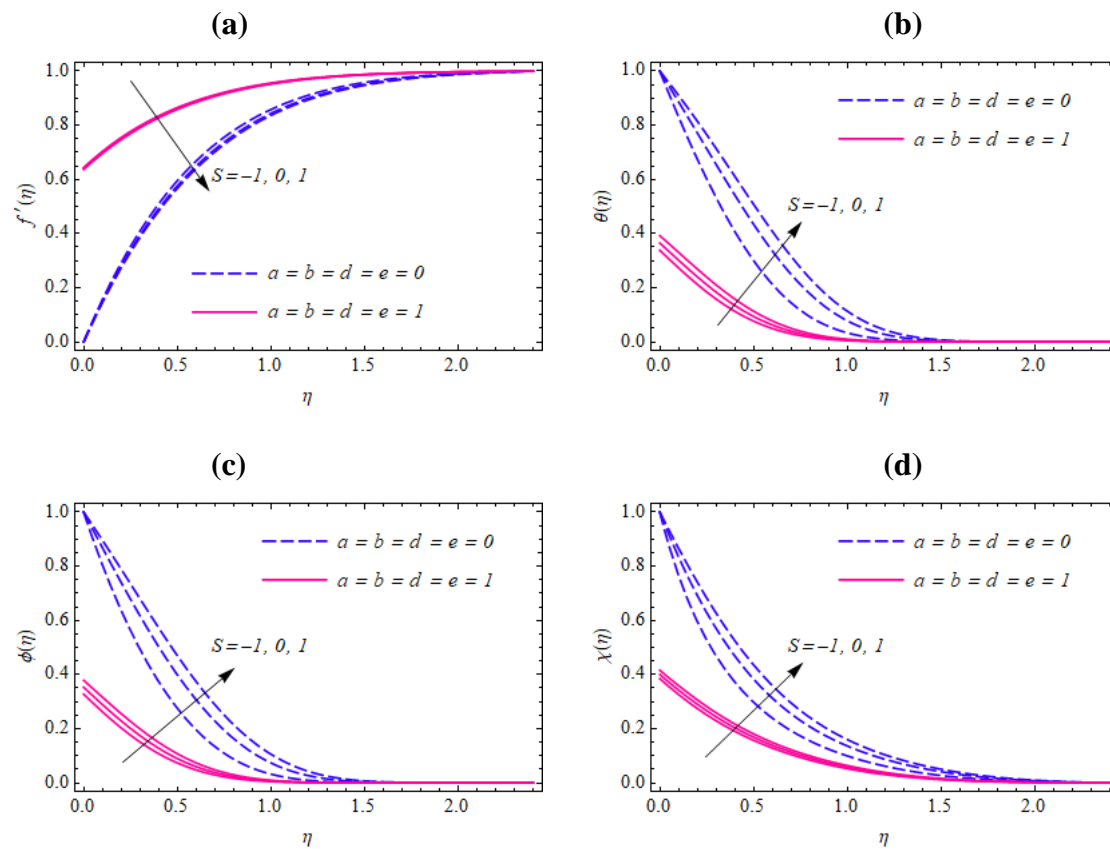


Fig. 2: Variation of $f'(\eta)$, $\theta(\eta)$, $\phi(\eta)$, and $\chi(\eta)$ with various values of S .

Fig. 2(c) depicts how the nanoparticle volume fraction vary with the change of blowing for both no-slip and slip boundary conditions. In both cases, a positive increment in S induces a rise in nanoparticle concentration, whereas a negative increment produces the reverse effect. Nanoparticle species boundary layer thickness is therefore enhanced with positive Stefan blowing but depleted with negative blowing. However, the modifications in nanoparticle concentration are much stronger for the no-slip (dotted) case. The case $S = 0$ corresponds to vanishing Stefan blowing. Faster convergence to the free stream is computed with the slip boundary condition case in contrast with the conventional noslip conditions.

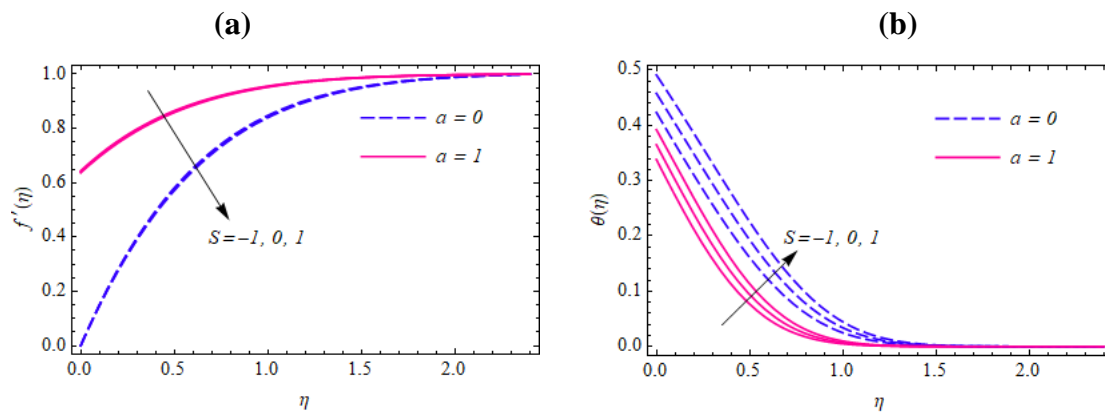
Fig. 2(d) plots the dimensionless motile microorganism profiles for variation in Stefan blowing again for both slip and without slip boundary conditions. Microorganism profiles are boosted with strong positive blowing from the wall, i.e., increasing nanoparticle boundary layer thickness. However, the opposite effect is produced with negative Stefan blowing. Microorganism propulsion in the nanofluid is only assisted with positive Stefan blowing, whereas swimming is inhibited with negative blowing. The distribution of microorganisms in

the coating boundary layer can be manipulated via modification in Stefan blowing, which is very useful from the materials processing viewpoint. As with other characteristics computed, the effect of Stefan blowing is much more dramatic without wall slip than with wall slip. In addition, the microorganism profiles again converge more slowly for the no-slip case relative to the slip case.

4.2 Impact of velocity slip

Fig. 3(a) establishes the influence of the blowing on the velocity *with and without velocity slip boundary conditions*. Here, the effects of Stefan blowing on the velocity profiles with and without velocity slip indicate no tangible change (single line), i.e., there is no discernible alteration in the velocity profiles. A similar outcome is also noticed in the case of no-slip boundary conditions. Effectively robust blowing at the wall does not affect the velocity profile; therefore, it does not change the momentum boundary layer thickness.

Fig. 3b shows an increasing trend of the temperature profiles with *positive* Stefan blowing parameter (S) but a decrement with *negative* S . The value of the temperature profile computed about 0.5 for the no-slip velocity boundary condition for an initial value of η ; however, these parameters were close to 0.4 for the slip velocity boundary condition. Increasing the velocity slip factor evidently induces a decrease of the temperature profiles for both solid wedge and permeable wedge and depletes the thermal boundary layer thickness.



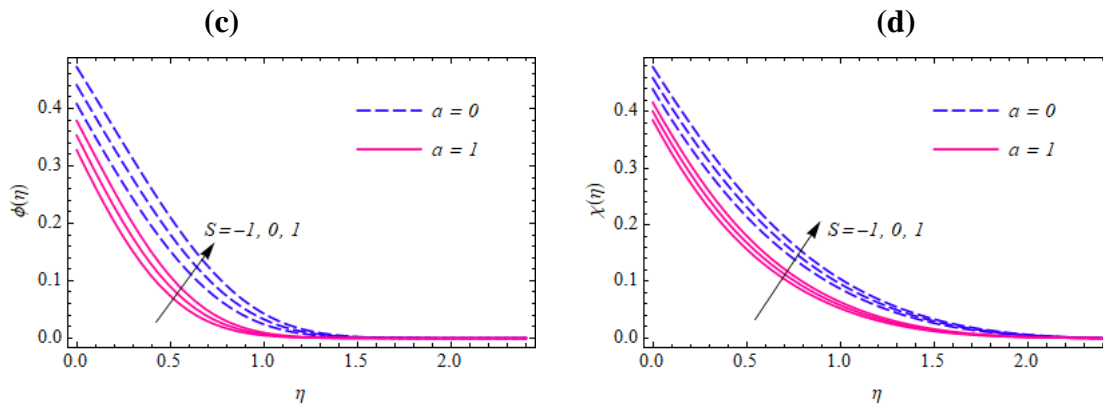


Fig. 3: Variation of $f'(\eta)$, $\theta(\eta)$, $\phi(\eta)$, and $\chi(\eta)$ for various values of S and α .

Fig. 3(c) plots the nanoparticle volume fraction profiles with the variation of the blowing parameter both in the presence and absence of velocity slip. The values of the concentration magnitudes are decreased with the negative blowing parameter but increased with positive blowing. Nanoparticle diffusion is therefore only assisted in the boundary layer regime with positive Stefan blowing, and a boost is produced in species boundary layer thickness. Higher magnitudes of nanoparticle concentration are computed without wall velocity slip compared with the case when slip is present. Therefore, nanoparticle diffusion is curbed with the wall slip. The inclusion of wall hydrodynamic slip is therefore critical in coating flow models since it more accurately predicts the velocity distributions. Without slip, velocity is clearly over-estimated.

The impacts of Stefan blowing on the motile microorganism number density is shown in Fig. 3(d). The positive blowing parameter enhances the microorganism profiles and produces a thicker microorganism concentration boundary layer. Negative blowing has the contrary effect. Significantly smaller microorganism concentration profiles are computed for the slip case. Again, including slip is important in modeling since it dampens the microorganism propulsion at the wedge surface (wall) and throughout the boundary layer regime. The implication is that when slip is present, the microorganism swimming is impeded in the regime.

4.3 Impact of temperature slip

Fig. 4(a) depicts the temperature profiles with temperature boundary slip conditions and variations of the Stefan blowing. Due to the positive values of the blowing, the temperature profiles became maximum, whereas they are minimized with negative Stefan blowing. Therefore, positive Stefan blowing clearly increases nanoparticle concentration boundary layer thickness. Furthermore, compared to the case when there is no temperature slip at the

wall ($b = 0$), the temperature profiles are depleted and result in a thinner boundary layer thickness when the temperature slip boundary condition ($b = 1$) is present. The temperature profile decay from the wedge surface in the absence of thermal slip is also much sharper compared with the case when thermal slip is present. Significant modification in temperature distribution is induced with thermal jump (slip) and Stefan blowing. Therefore, these effects are important to include in more realistic models of boundary layer coating systems.

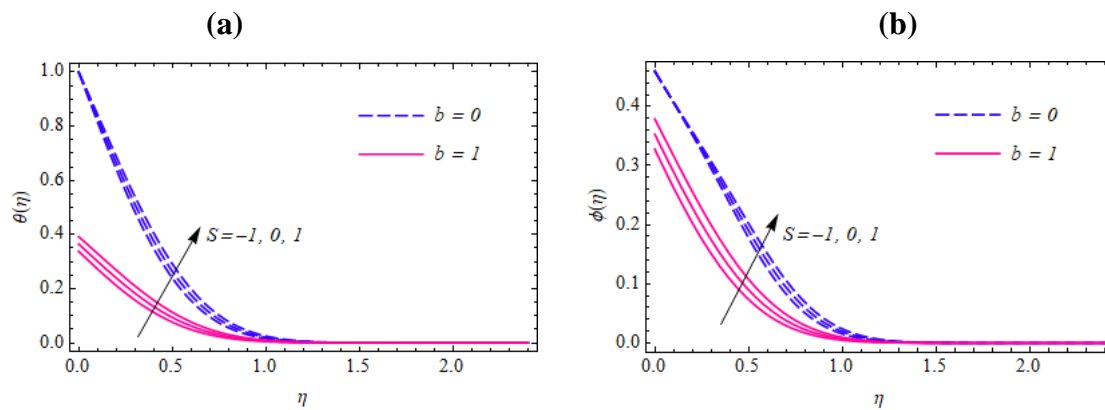


Fig. 4: Variation of $\theta(\eta)$ and $\phi(\eta)$ for various values of S and b .

The blowing effects on the nanoparticle volume fraction is displayed in Fig. 4(b). For no-slip temperature boundary condition, the wall (wedge surface) values of the number density are invariant. Increasing the positive Stefan blowing parameter boosts the microorganism number density, whereas negative Stefan blowing depletes it. The case of a solid wedge surface ($S = 0$) falls between these two extremes. Much smaller microorganism density number values are associated with the temperature slip case ($b = 1$) and a spread of values at the wall, unlining the no slip case.

4.4 Impact of mass slip

Fig. 5(a) illustrates the influences of the nanoparticle volume fraction slip parameter and the Stefan blowing parameter on the velocity. The effect of the positive Stefan blowing parameter caused a much more significant decrement in nanoparticle concentration in the no-slip case compared with the slip case. A slight reduction in velocity for both cases is observed. Higher values are computed for the negative Stefan blowing parameter, and nanoparticle concentration boundary layer thickness is boosted. The presence of nanoparticle

concentration slip ($d = 1$) manifests in a much thinner nanoparticle boundary layer thickness for either the permeable or solid wedge.

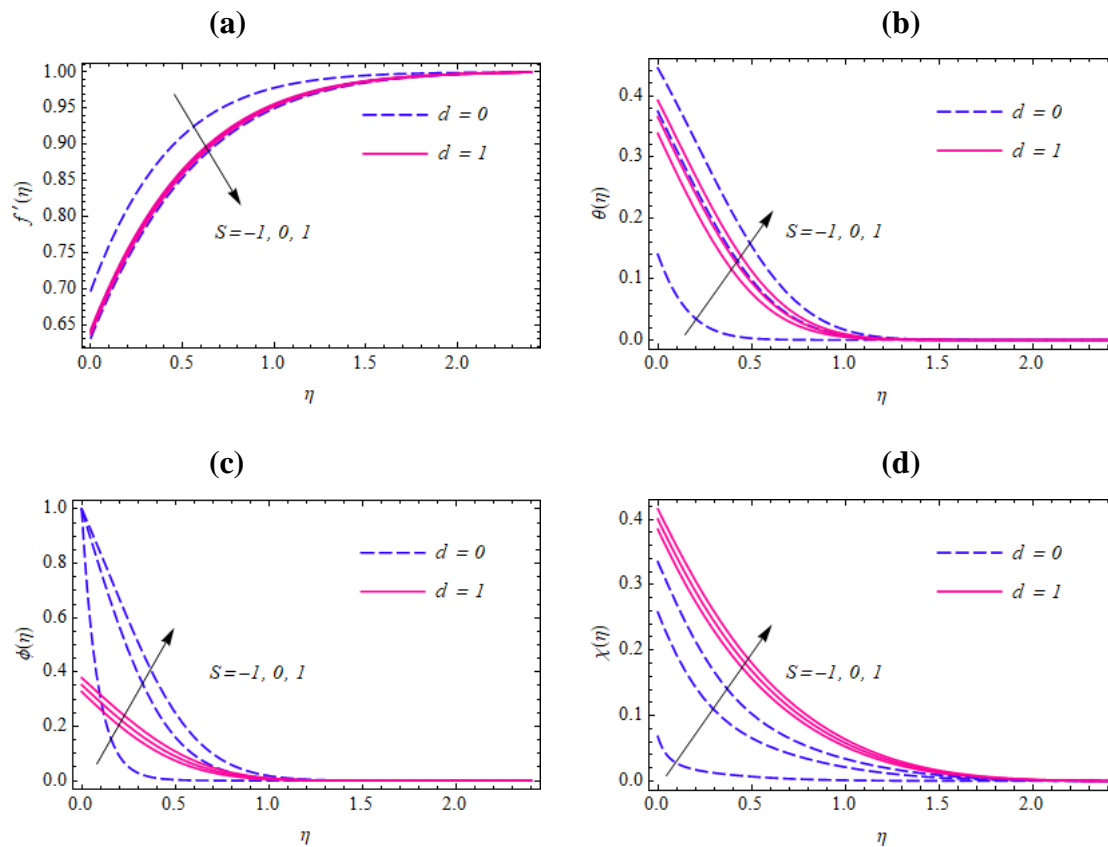


Fig. 5: Variation of $f'(\eta)$, $\theta(\eta)$, $\phi(\eta)$, and $\chi(\eta)$ for various S and d .

Fig. 5(b) depicts the variations of the blowing and nanoparticle volume fraction slip on the temperature. Increasing the positive blowing parameter (blowing to the wall) clearly boosts the temperature for both the slip and no slip cases. Much higher magnitudes are computed in the no-slip case ($d = 0$). However, the negative blowing parameter induces a reduction in temperature and also thermal boundary layer thickness. Overall, blowing to the wall enhances temperature and thermal diffusion, whereas blowing from the wall reduces it. The rapid convergence of the temperature profiles is observed in the vicinity of $\eta = 1.1$ for both cases.

Fig. 5(c) shows the effects of blowing on the nanoparticle volume fraction for various nanoparticle mass slip parameter. With nanoparticle mass slip present, concentration magnitudes are significantly suppressed, especially near the wedge surface (wall). Nanoparticle species boundary layer thickness is generally reduced with negative Stefan blowing but accentuated with positive Stefan blowing.

Fig. 5(d) prescribes the impacts of the motile microorganism density number for the microorganism concentration slip and the Stefan blowing parameter variation. In the existence of the microorganism slip, the microorganism profiles are maximized for both blowing directions (positive and negative Stefan parameters). However, higher values are achieved with a positive Stefan parameter. In the absence of microorganism slip, a substantial reduction is computed in microorganism density number throughout the boundary layer, and the microorganism species boundary layer thickness is also depleted.

4.5 Impacts of micororganism slip

Fig. 6(a) illustrates the development of the nanoparticle volume fraction with the different values of blowing and microorganism slip parameters. The topology of the concentration profiles is almost indistinguishable from the temperature profiles with a change in the slip effect ($e = 0, 1$), which is logical since there is no interaction between nanoparticles and swimming microorganisms in the regime. In other words, the microorganism slip does not influence the nanoparticle concentration distribution. However, there is a distinct elevation in nanoparticle concentration profiles with positive Stefan blowing and a depletion with negative Stefan blowing. Nanoparticle boundary layer thickness, as indicated earlier, is therefore increased with positive Stefan blowing.

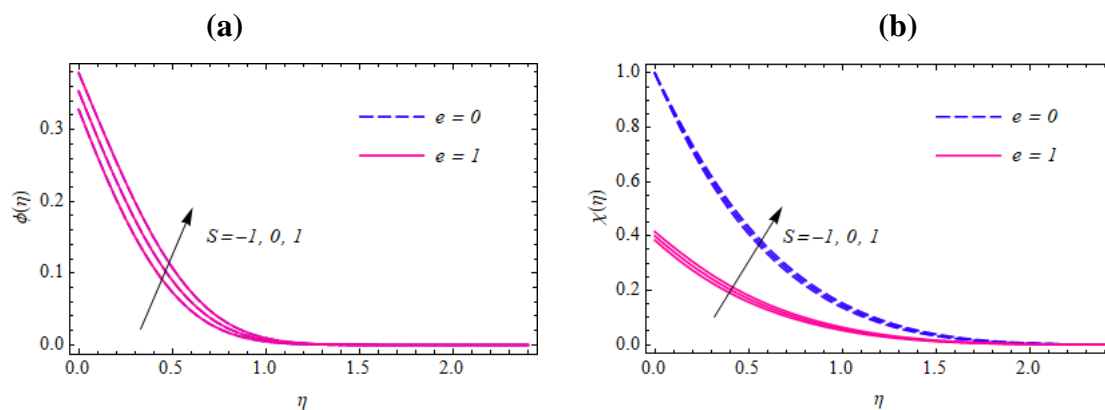


Fig. 6: Variation of $\phi(\eta)$ and $\chi(\eta)$ for various values of S and e .

Fig. 6(b) presents the influence of the blowing and microorganism slip parameters on the motile microorganism density number function. The microorganism profiles are strongly amplified with the blowing from the wall. The microorganism profiles are depleted with increasing microorganism slip at the wedge surface ($e = 1$) since this induces a delay in swimming. Much greater microorganism species boundary layer thickness corresponds to the

non-slip case. Very smooth monotonic decays are computed from the wall to the potential flow.

4.6 Influence of Lewis number

Fig. 7(a) reveals the impacts of the blowing and the Lewis number on the dimensionless temperature profiles. Here, as Lewis number increases from 1 to 2 (and nanoparticle diffusivity is reduced, $Le = \frac{\alpha}{D_H}$), the temperature is decreased. The conductive heat transfer is reduced with lower molecular diffusivity of the nanoparticles, which manifests in a decrease in thermal boundary layer thickness. With the positive Stefan blowing parameter, the temperature profiles are elevated whereas they are suppressed with negative blowing. Maximum temperature is computed for $Le = 1$ (equivalent thermal and nanoparticle mass diffusivities) and $S = 1$.

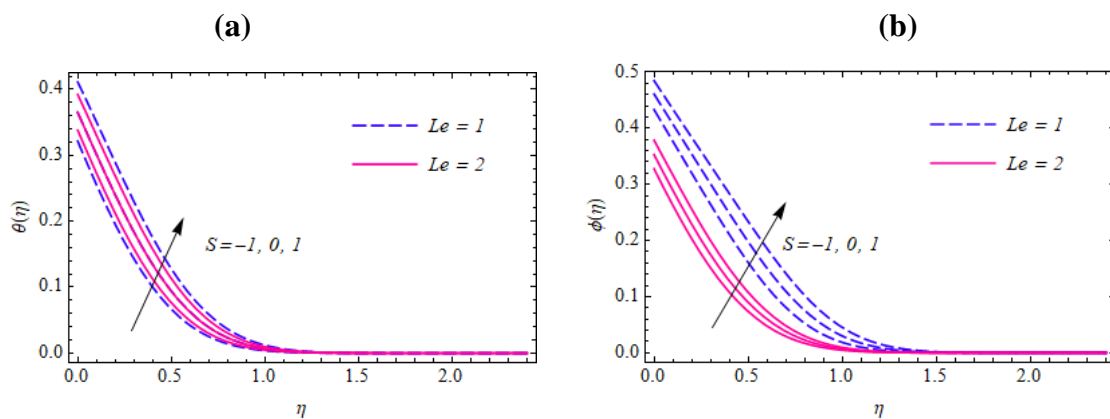


Fig. 7: Variation of $\theta(\eta)$ and $\phi(\eta)$ for various values of S and Le .

Fig. 7(b) shows the nanoparticle concentration profile variation with the Lewis number and blowing parameter variation. Concentration profiles for the nanoparticle species are depleted with strong blowing to the wall (negative S) and a superior Lewis number ($Le = 2$). The concentration profiles are enhanced for strong blowing to the wall ($S = 1$) at a lower Lewis number ($Le = 1$). Therefore, nanoparticle boundary layer thickness is boosted only for positive Stefan blowing and lower Lewis number.

4.7 Effects of the magnetic field

Fig. 8(a) reveals the impact of magnetic field with the blowing on the velocity. Magnetic parameter induces significant elevation of the flow due to the free stream effect. Therefore,

the flow is accelerated with a stronger magnetic field, not damped as in conventional magnetohydrodynamic boundary layer flows. The *electrically non-conducting* case ($M = 0$), which corresponds to a vanishing magnetic field, produces deceleration, although reverse flow is not computed (no negative velocity values). A greater magnetic field via the Lorentz body force effect reduces momentum boundary layer thickness, confirming the external magnetic field's excellent ability to manipulate flow characteristics in boundary layer coating flows. However, the effects of blowing are trivial with a strong magnetic field ($M = 2$), whereas they do induce some modification for the non-conducting case ($M = 0$). There is a slight increment in velocity with negative Stefan blowing ($S = -1$) and a decrease with positive blowing ($S = 1$) for the non-magnetic scenario. Therefore, momentum (hydrodynamic) boundary layer thickness is reduced for negative Stefan blowing and enhanced for positive Stefan blowing.

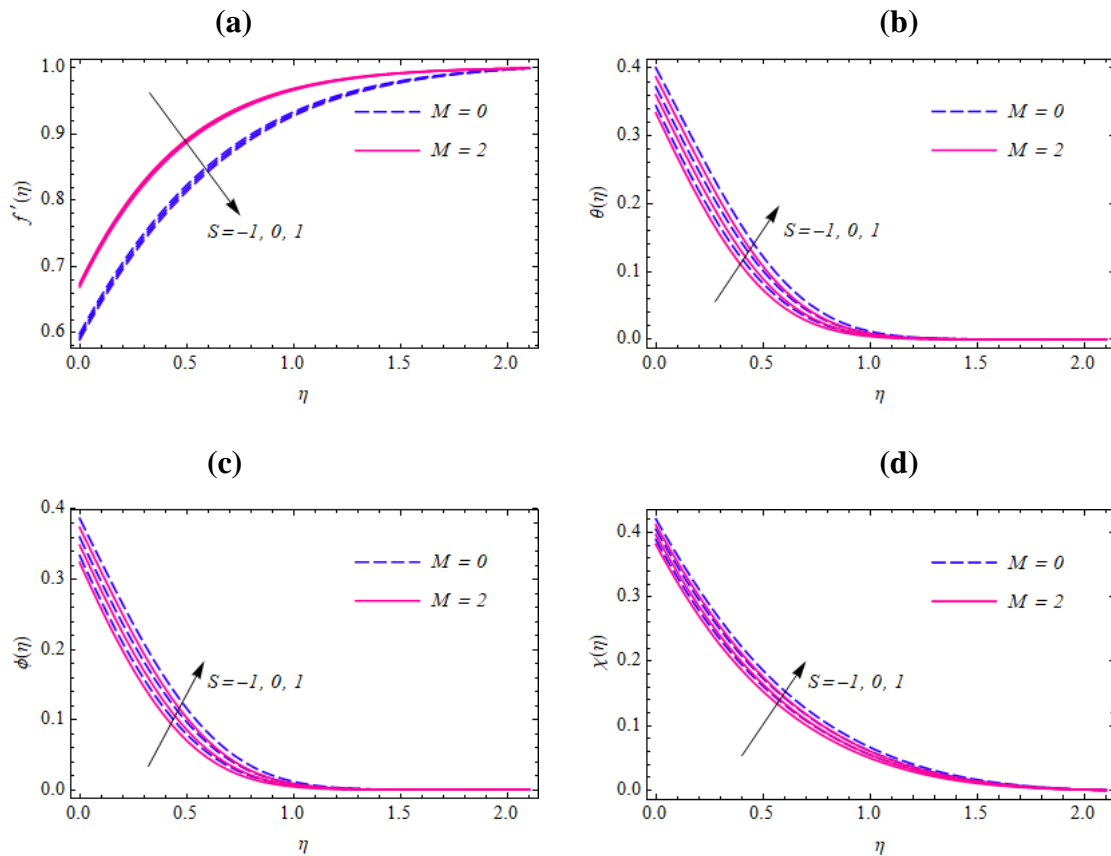


Fig. 8: Variation of $f'(\eta)$, $\theta(\eta)$, $\phi(\eta)$, and $\chi(\eta)$ for various values of S and M .

Fig. 8(b) illustrates how the temperature profiles respond when the combined effects of the Stefan blowing and magnetic field are applied. It is found that, temperature enhances when $S > 0$ and reverse trend is noticed for $S < 0$. Increasing the magnetic field reduces the dimensionless temperature weakly. This is the converse effect to conventional MHD

boundary layer flows. The free stream effect implies that less work is required in moving the nanofluid as the Lorentz body force does not induce retardation but rather is assistive. Therefore, thermal energy is not dissipated; it is conserved. This cools the regime and manifests in lower temperatures and a thinner thermal boundary layer thickness.

Fig. 8(c) describes the distribution of the nanoparticle concentration profiles with the magnetic field variation for different values of the blowing parameter. The concentration profiles are quite similar to the temperature profiles. A stronger magnetic field slightly decreases nanoparticle concentration, which is also decreased with negative Stefan blowing (blowing to the wall). However, positive blowing elevates the nanoparticle species' concentration, which is also achieved with a vanishing magnetic field. Again, excellent manipulation of nanoparticle distribution in the boundary layer is possible with reasonable combinations of the magnetic field applied and the Stefan blowing imposed.

The combined influence of the magnetic field and blowing on the motile microorganism profiles is shown in Fig. 8(d). Motile microorganism profiles were marginally decreased with the increase of the magnetic field and also with strong blowing to the wall (negative Stefan blowing parameter). Microorganism density number is conversely boosted for the non-magnetic case and with strong blowing from the wall (positive Stefan blowing), and microorganism species boundary layer thickness is also increased.

4.8 Effects of bioconvection Lewis number and bioconvection Péclet number

Fig. 9(a) presents the belongings of the bioconvection Lewis number and blowing parameter on the dimensionless motile microorganism profiles. Bioconvection Lewis number, $Lb = \frac{\nu}{D_n}$ expresses the ratio of kinematic viscosity to the molecular diffusivity of microorganisms. So, increasing the diffusivity of microorganisms reduces the bioconvection Lewis number. Therefore, decreased bioconvection Lewis number enhances motile microorganism density number values. Positive Stefan blowing parameter also boosts microorganism density number values and elevates the microorganism boundary layer thickness. Effectively, strong blowing from the wall with lower bioconvection Lewis number results in maximum magnitudes of microorganism density number, whereas the contrary behavior is observed for strong blowing to the wall (negative Stefan blowing) with higher Lb .

Fig. 9(b) demonstrates the variation of the motile microorganism density number with bioconvection Péclet number and blowing parameters. Note that bioconvection Péclet number is the ratio between constant maximum cell swimming speed and diffusivity of microorganisms. Therefore, the bioconvection Péclet number has had pronounced effects on the dimensionless motile microorganism profiles. Microorganism density number is reduced with an increase in this parameter since the molecular diffusivity of the microorganisms is reduced. This inhibits their swimming intensity and also produces a decrement in microorganism species boundary layer thickness. With blowing to the wall (negative Stefan blowing parameter), microorganism density numbers are also suppressed, whereas they are boosted with positive Stefan blowing (blowing away from the wall). Therefore, microorganism boundary layer thickness is greater with positive Stefan blowing and a lower Péclet number. The selection of appropriate gyrotactic species is required to manipulate the Péclet number, which can be used to regulate coating constitution characteristics on the wedge.

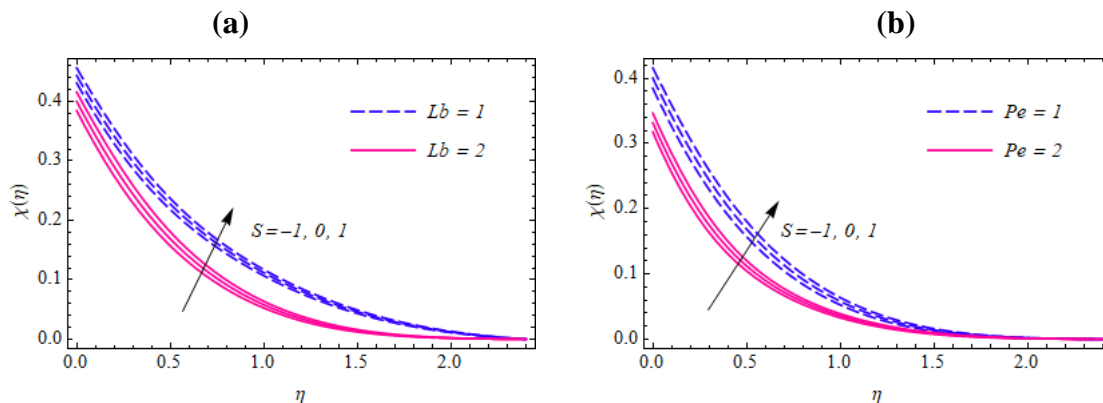


Fig. 9: Variation of $\chi(\eta)$ for various values of S , Lb , and Pe .

4.9 Effects of Hartree wedge parameter

Fig. 10(a) displays the influences of the wedge (m) and the blowing parameter (S) on the velocity. The wedge parameter, $m = \beta/(2 - \beta)$, is also known as the Hartree pressure gradient parameter, which corresponds to a wedge apex angle of $\pi \beta$ as shown in **Fig. 1**. When $m = 0$ we have the classical case of Blasius boundary layer flow on a flat plate. In contrast, when $m = 1$, we have the case of Hiemenz stagnation flow. For the case of $m < 0$, adverse pressure gradient effects arise, which may lead to boundary layer separation

on the wedge, and therefore, this scenario is not considered. A much greater velocity is computed for $m = 1$ compared to $m = 0$. In other words, flow acceleration (thinner momentum boundary layer) is produced for the former, and flow deceleration (thicker momentum boundary layer) corresponds to the latter. Stefan blowing does not influence the Hiemenz stagnation flow case ($m = 1$). However, for the Blasius flow case ($m = 0$), negative Stefan blowing produces a slight acceleration, whereas positive Stefan blowing manifests in a weak deceleration.

Fig. 10(b) represents the impact of the wedge and blowing parameters on the temperature profiles. When $m = 1$, the temperature profiles are reduced, whereas, for $m = 0$, they are enhanced. Therefore, heating is produced in the Blasius flow case, whereas cooling is induced in the Hiemenz stagnation flow case. Increased positive Stefan blowing boosts the temperature and thermal boundary layer thickness, whereas negative Stefan blowing induces the contrary response.

Fig. 10(c) discloses the impact of of the wedge and blowing on the nanoparticle volime fraction. A similar pattern is computed with temperatures. Blasius flow ($m = 0$) corresponds to higher nanoparticle concentration, whereas Hiemenz stagnation flow ($m = 1$) is associated with lower concentration magnitudes (thinner species boundary layer thickness). Positive Stefan blowing parameter also enhances the concentration of nanoparticles, whereas negative blowing produces the opposite effect.

Fig. 10(d) determines the profiles of motile microorganisms under varying wedge parameter settings and Stefan blowing parameter variations. The motile microorganism density numbers are enhanced when $m = 0$ (Blasius flow) but reduced for the Hiemenz case ($m = 1$). Therefore, the wedge geometry has a profound effect on the microorganism distribution. A much thinner microorganism boundary layer thickness is produced when $m = 1$ compared with $m = 0$. Therefore, a simple manipulation in the apex angle can be exploited to control the microorganism's behavior in the nanofluid coating significantly.

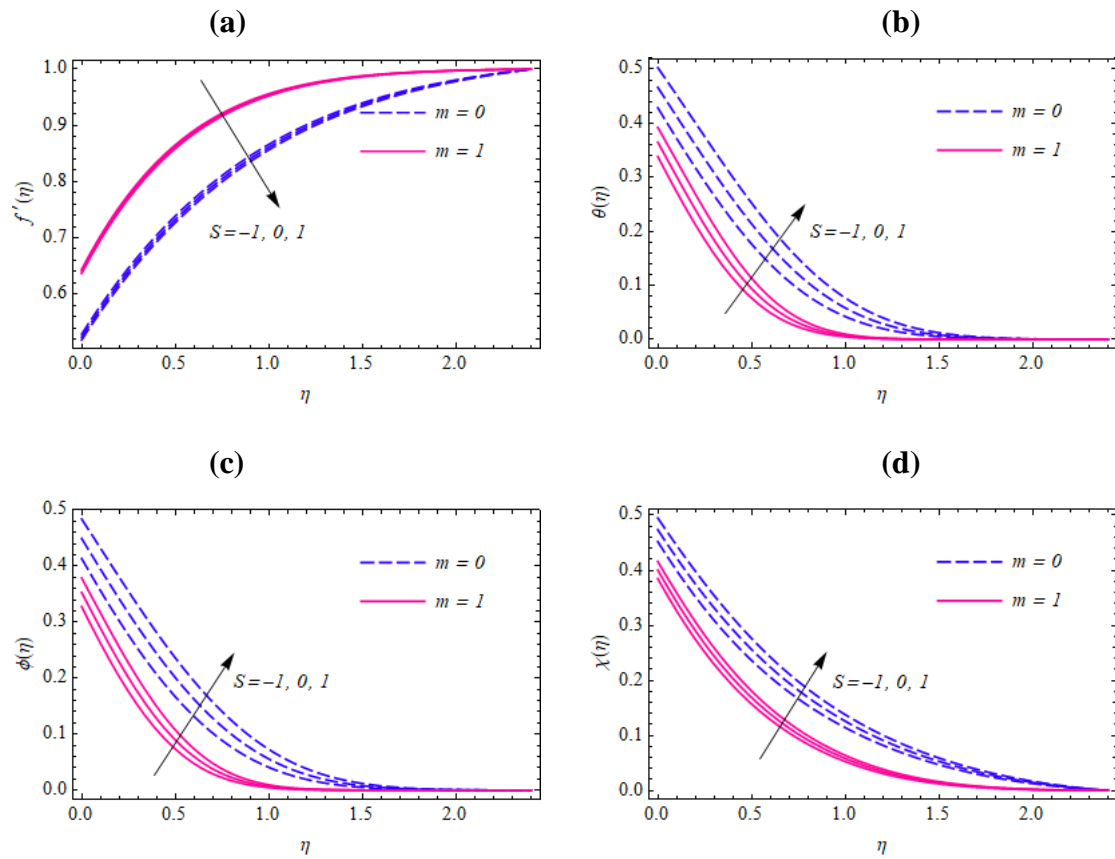


Fig. 10: Variation of $f'(\eta)$, $\theta(\eta)$, $\phi(\eta)$, and $\chi(\eta)$ for various values of S and m .

Positive Stefan blowing (blowing from the wall) also boosts the density number of motile microorganisms, whereas negative Stefan blowing (away from the wall) suppresses values and decreases the microorganism species boundary layer thickness.

4.10 Shear stress

Fig. 11(a) demonstrates the manners of the shear stress $f'''(0)$ for change of the blowing, magnetic field, and velocity slip parameters.

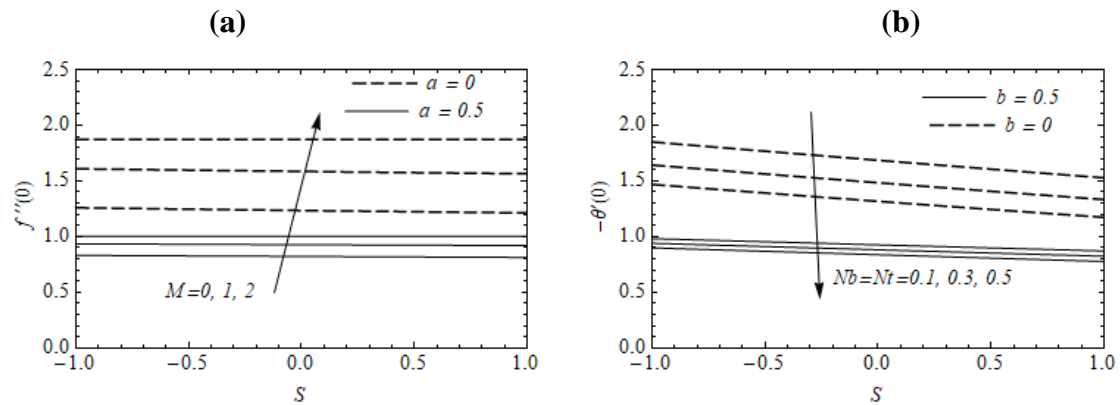


Fig. 11(a): Variation of the shear stress for the different values of S, M , and α .

Variation of the heat transfer gradient for the different values of S, Nt, Nb , and b .

Fig. 11(b):

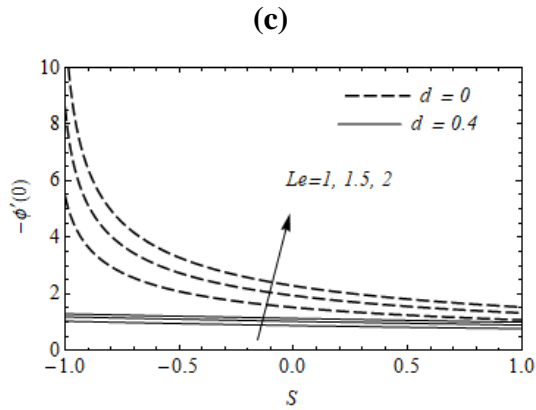


Fig. 11(c): Variation of the local nanoparticle concentration gradient for different values of S, Le , and d .

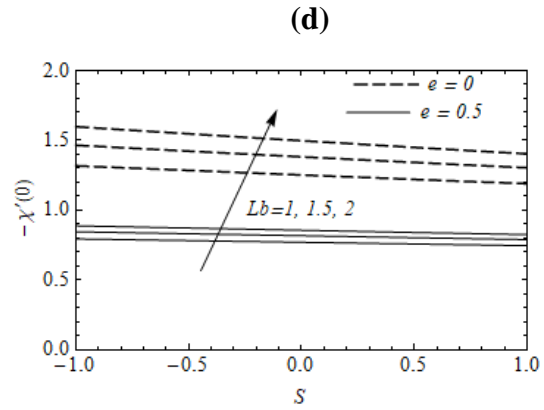


Fig. 11(d): Variation of the local microorganism number density gradient for different values of S, Lb , and e .

Skin friction was observed to increase very weakly in a linear fashion with a positive blowing since velocity profiles very slightly decrease with the increasing of blowing parameter. On the other hand, the magnetic field parameter induces strong acceleration on the wedge surface and produces a much thinner velocity boundary layer. Skin friction (dimensionless shear stress) is therefore enhanced with the increasing magnetic field strength and without velocity slip ($\alpha = 0$). Skin friction is strongly reduced with increased velocity (momentum) wall slip ($\alpha = 0.5$).

Fig. 11(b) displays the heat transfer gradient at the wall owing to a change in the blowing, thermal slip, and the two nanoscale parameters featured in the Buongiorno model, i.e., Brownian motion and thermophoresis parameters. The positive Stefan blowing parameter reduces the heat transfer rate at the wedge surface since it increases temperatures within the boundary layer and inhibits thermal energy transfer to the wedge face. Therefore, strong blowing from the wall increases thermal boundary layer thickness, whereas negative Stefan blowing, i.e., *strong blowing to the wall*, reduces temperature and thermal boundary layer thickness. Negative blowing generates a greater local Nusselt number at the wall (wedge surface), and positive blowing lowers it. Greater temperature slip reduces heat transfer rate,

i.e., Nusselt numbers become more negative. $-\theta'(0)$ is also strongly reduced with increasing Brownian motion parameter and thermophoresis parameter since both these nanoscale effects heat the boundary layer and increase temperatures due to respective actions of enhanced ballistic collisions and a driving thermal gradient. This suppresses heat transfer to the wedge surface and depletes the Nusselt number.

The behavior of the nanoparticle volume fraction gradient at the wedge wall with blowing parameter and Lewis number is shown in Fig. 11(c). It is observed that the mass transfer rates were massively boosted for strong blowing to the wall (negative Stefan parameter). In contrast, the opposite effect is induced with blowing from the wall (positive Stefan parameter). With $Le = 2$ and the absence of nanoparticle mass slip ($d = 0$), the local mass transfer rate is markedly increased. It is clear that with the higher values of the Lewis number and the negative value of the blowing parameter, maximum values of the local Sherwood number are produced. Consequently, strong blowing to the wedge wall with the help of a higher Lewis number produces greater local mass transfer rates. However, with blowing *from the wedge wall*, a contrary effect on mass transfer is induced, i.e., it is depleted and also in the absence of concentration boundary slip. However, in the presence of slip, the local mass transfer variation is linear, and only a weak modification is observed with the Stefan blowing parameter. The nanoparticle volume fraction slip strongly depresses the mass transfer rate. The local Sherwood number is enhanced with a higher Lewis number. Since the Lewis number is inversely proportional to the Brownian diffusion coefficient and directly proportional to thermal diffusivity, the higher Lewis number depletes nanoparticle concentration profiles. As a result, nanoparticles' migration from the boundary layer to the wedge surface is increased, producing a boost in local mass transfer rates with higher Lewis numbers.

Fig. 11(d) shows that enhancing bioconvection Lewis number elevates the local microorganism transfer rate $-\chi'(0)$ and increasing the positive Stefan blowing parameter and microorganism slip factor depletes the microorganism transfer rate. A positive higher blowing parameter increases microorganism boundary layer thickness, inhibiting microorganisms swimming to the wedge surface. This reduces the microorganism density number gradient at the wall. The presence of microorganism slip also reduces the microorganism transfer rate at the wedge wall. The microorganism wall density number

gradient is increased when no microorganism slip boundary conditions are imposed. Increasing bioconvection Lewis number also implies lower molecular diffusivity of microorganisms, resulting in an enhanced microorganism transfer rate at the surface of the wedge.

5. Conclusions

As a simulation of magnetohydrodynamic (MHD) coating flow with smart functional bioconvective nanoliquids, a mathematical model has been described for the external boundary layer Falkner-Skan flow of an electroconductive nanofluid containing gyrotactic microorganisms on a two-dimensional wedge with blowing and multiple slip the wedge wall. Buongiorno's two-component nanoscale formulation has been adopted. The model has been formulated using a system of partial differential equations and appropriate boundary conditions, which were then transformed into a set of similarity equations with appropriate similarity variables. The non-dimensional boundary value problem has been solved numerically with the aid of the Mathematica software solver package named "NDSolve" using a finite element modification. The impacts of the controlling parameter on key transport characteristics, i.e., dimensionless velocity, temperature, nanoparticle species concentration (volume fraction), microorganism density number (concentration), skin friction coefficient, local heat transfer rate (local Nusselt number), local mass transfer rate (local Sherwood number) and the microorganism local density number gradient are computed and visualized graphically. The special cases of Blasius flow and Hiemenz stagnation flow are also studied by carefully prescribing the wedge parameter (Hartree pressure gradient parameter). Numerical solutions have been validated with previous literature. The principal findings are highlighted as follows:

- (i) Positive blowing parameter reduces skin friction, whereas increasing the magnetic field elevates it due to the free stream effect in Falkner-Skan wedge flow.
- (ii) Increasing thermophoresis and Brownian motion parameters diminish the heat transfer rate at the wall (Nusselt number).
- (iii) Increasing the positive Stefan blowing parameter reduces the Nusselt number at the wedge surface.
- (iv) Increasing bioconvection Lewis number strongly elevates the nanoparticle mass transfer rate (Sherwood number) at the wall for negative Stefan blowing but reduces it

for positive Stefan blowing in the absence of nanoparticle concentration slip boundary conditions.

- (v) Bioconvection Lewis number enhances local microorganism density number gradient in the absence of microorganism slip compared to when this slip effect is present.
- (vi) Increasing negative Stefan blowing at the wall (wedge surface) slowly increases the local microorganism transfer rate.
- (vii) Increasing the magnetic field slightly reduces temperature and thermal boundary layer thickness and depletes the nanoparticle concentration and microorganism density magnitudes.
- (viii) Hydrodynamic boundary layer thickness is reduced for negative Stefan blowing and enhanced for positive Stefan blowing for the non-magnetic case.

The outcomes of this study may provide useful insights into the optimized design of functional nanofluid coatings doped with gyrotactic microorganisms. However, the model presented has been Newtonian. Future work may address non-Newtonian behavior using a range of robust rheological models, e.g., micropolar models [57], and also consider other effects such as unsteady flow with variable thermophysical properties and carbon nanotubes (CNTs) [58]. Additionally non-Darcy porous media [59] and non-Fourier thermophysical effects [60] may also be addressed in subsequent studies.

References

- [1] Maxwell, J. C., *Treatise on Electricity and Magnetism*, vol. 1, Oxford: Clarendon Press, 1873.
- [2] Choi, S., "Enhancing thermal conductivity of fluids with nanoparticles, developments and applications of non-Newtonian flows," *ASME Fluids Engineering Division*, vol. 66, pp. 99-105, 1995.
- [3] Lee, C. E., "Rapid and repeated invasions of fresh water by the saltwater Copepod *Eurytemora Affinis*," *Evolution*, vol. 53, no. 5, pp. 1423–1434, 1999.
- [4] Murshed, S. M. S., Leong, K. C., and Yang, C., "Thermophysical and electrokinetic properties of nanofluids—a critical review," *Applied Thermal Engineering*, vol. 28, no. 17-18, pp. 2109-2125, 2008.
- [5] Kakaç, S., Özerinç, S., and Yazıcıoğlu, A. G., "Enhanced thermal conductivity of nanofluids: a state-of-the-art review," *Microfluids and Nanofluids*, vol. 8, no. 2, pp. 145-170, 2010.

- [6] Kaufui V. W., and Omar, D. L., "Applications of Nanofluids: Current and Future," *Advances in Mechanical Engineering*, vol. 2, 2010.
- [7] Falkner, V. M., and Skan, S. W., "Some approximate solutions of the boundary-layer equations," *Philosophical Magazine*, vol. 12, pp. 865-896, 1931.
- [8] S. A.Gaffar, V. R. Prasad, B. Vijaya and O. Anwar Bég, Mixed convection flow of magnetic viscoelastic polymer from a non-isothermal wedge with Biot number effects, *Int. J. Engineering Mathematics*, Volume 2015, Article ID 287623, 15 pages (2015).
- [9] O. Anwar Bég, B. Vasu, Atul Kumar Ray, T.A. Bég, Ali Kadir, Henry J. Leonard and R.S.R. Gorla, Homotopy simulation of dissipative micropolar flow and heat transfer from a two-dimensional body with heat sink effect: applications in polymer coating, *Chem. Biochem. Eng. Quart.* 34 (4) 257–275 (2020).
- [10] J. Zueco, O. Anwar Bég, Network simulation solutions for laminar radiating dissipative magneto-gas dynamic heat transfer over a wedge in non-Darcian porous regime, *Mathematical and Computer Modelling*, 50, 3-4, 439-452 (2009).
- [11] F. T. Zohra, M.J. Uddin and A.I. Ismail and O. Anwar Bég, Bioconvective electromagnetic nanofluid transport from a wedge geometry: simulation of smart electro-conductive bio-nano-polymer processing, *Heat Transfer*, 47, 231-250 (2018).
- [12] Lee, S. Y., and Kim, H. U., "Systems strategies for developing industrial microbial strains," *Nature Biotechnology*, vol. 33, no. 10, pp. 1061-1072, 2015.
- [13] Shaw, S., Sibanda, P., Sutradhar, A., and Murthy, P. V. S. N., "Magnetohydrodynamics and Soret effects on bioconvection in a porous medium saturated with a nanofluid containing gyrotactic microorganisms," *ASME Journal of Heat Transfer*, vol. 136, no. 5, pp. 52601, 2014.
- [14] Zaimi, K., Ishak, A., and Pop, I., "Stagnation-point flow toward a stretching /shrinking sheet in a nanofluid containing both nanoparticles and gyrotactic microorganisms," *ASME Journal of Heat Transfer*, vol. 136, no. 4, pp. 041705, 2014.
- [15] Xu, H., and Pop, I., "Fully developed mixed convection flow in a horizontal channel filled by a nanofluid containing both nanoparticles and gyrotactic microorganisms," *European Journal of Mechanics B Fluids*, vol. 46, pp. 37-45, 2014.
- [16] Raees, A., Xu, H., Sun, Q., and Pop, I., "Mixed convection in gravity-driven nano-liquid film containing both nanoparticles and gyrotactic microorganisms," *Applied Mathematics and Mechanics*, vol. 36, no. 2, pp. 163-178, 2015.
- [17] G. Kumaran, R Sivaraj, V. Ramachandra Prasad, O. Anwar Bég, Numerical study of axisymmetric magneto-gyrotactic bioconvection in non-Fourier tangent hyperbolic nano-functional reactive coating flow of a cylindrical body in porous media, *European Physical Journal Plus*, 136, 1107 (2021). <https://doi.org/10.1140/epjp/s13360-021-02099-z>. (32 pages)

- [18] O. Anwar Bég, Nonlinear multi-physical laminar nanofluid bioconvection flows: Models and computation, A. Sohail, Z. Li (Eds.): *Computational Approaches in Biomedical Nano-Engineering*, Wiley, Chapter 5, pp. 113-145 (2018).
- [19] Busila, M. *et al.*, Antibacterial and photocatalytic coatings based on Cu-doped ZnO nanoparticles into microcellulose matrix. *Materials*, 15, 7656 (2022).
- [20] Mitra, D.; Kang, E.T.; Neoh, K.G., Antimicrobial copper-based materials and coatings: potential multifaceted biomedical applications. *ACS Appl. Mater. Interfaces*, 12, 21159–21182 (2020).
- [21] Taylor, E. N., and Webster, T. J., The use of superparamagnetic nanoparticles for prosthetic biofilm prevention. *Int. J. Nanomed.* 4, 145–152 (2009).
- [22] Akbar, N. S., and Khan, Z. H., "Magnetic field analysis in a suspension of gyrotactic microorganisms and nanoparticles over a stretching surface," *Journal of Magnetism and Magnetic Materials*, vol. 410, pp. 72-80, 2016.
- [23] Mutuku, W. N., and Makinde, O. D., "Hydromagnetic bioconvection of nanofluid over a permeable vertical plate due to gyrotactic microorganisms," *Comp. Fluids*, vol. 95, pp. 88-97, 2014.
- [24] Xu, H., "Lie group analysis of a nanofluid bioconvection flow past a vertical flat surface with an outer power-law stream," *ASME Journal of Heat Transfer*, vol. 137, no. 4, pp. 041101.1-041101.9, 2015.
- [25] Amirson, N. A., Uddin, M. J., and Ismail, A. I., "Three-dimensional stagnation point flow of bionanofluid with variable transport properties," *Alexandria Engineering Journal*, vol. 55, no. 3, pp. 1983–1993, 2016.
- [26] Latiff, N. A., Uddin, M. J., and Ismail, A. I. M., "Stefan blowing effect on bioconvective flow of nanofluid over a solid rotating stretchable disk," *Propulsion and Power Research*, vol. 5, no. 4, pp. 267–278, 2016.
- [27] Babu, M. J., and Sandeep, N., "Effect of nonlinear thermal radiation on non-aligned bioconvective stagnation point flow of a magnetic-nanofluid over a stretching sheet," *Alexandria Engineering Journal*, vol. 55, no. 3, pp. 1931–1939, 2016.
- [28] Makinde, O. D., and Animasaun, I. L., "Thermophoresis and Brownian motion effects on MHD bioconvection of nanofluid with nonlinear thermal radiation and quartic chemical reaction past an upper horizontal surface of a paraboloid of revolution," *Journal of Molecular Liquids*, vol. 221, pp. 733–743, 2016.
- [29] Uddin, M. J., Kabir, M. N., Bég, O. A., and Alginahi, Y., "Chebyshev collocation computation of magneto-bioconvection nanofluid flow over a wedge with multiple slips and magnetic

- induction," *Proceedings of the Institution of Mechanical Engineers, Part N: Journal of Nanomaterials, Nanoengineering and Nanosystems*, vol. 232, no. 4, pp. 109-122, 2018.
- [30] Uddin, M. J., Khan, W. A., Qureshi, S. R., and Bég, O.A., "Bioconvection nanofluid slip flow past a wavy surface with applications in nano-biofuel cells," *Chinese Journal of Physics*, vol. 55, no. 5, pp. 2048-2063, 2017.
- [31] Nellis, G., and Klein, S., *Heat Transfer*, 1st ed., Cambridge University Press, pp. 974-978, 2008.
- [32] Lienhard, IV J. H., and Lienhard, V J. H., *A Heat Transfer Textbook*, 3rd ed., Massachusetts: Phlogiston Press, pp. 662–663, 2005.
- [33] Fang, T., "Flow and mass transfer for an unsteady stagnation-point flow over a moving wall considering blowing effects," *ASME Journal of Fluids Engineering*, vol. 136, no. 4, pp. 071103, 2014.
- [34] Fang, T., and Jing, W., "Flow, heat, and species transfer over a stretching plate considering coupled Stefan blowing effects from species transfer," *Communication in Nonlinear Science and Numerical Simulation*, vol. 19, no. 9, pp. 3086–3097, 2014.
- [35] Latiff, N. A., Uddin, M. J., and Ismail, A. I. M., "Stefan blowing effect on bioconvective flow of nanofluid over a solid rotating stretchable disk," *Propulsion and Power Research*, vol. 5, no. 4, pp. 267–278, 2016.
- [36] Uddin, M. J., Bég, O. A., and Bég, T. A., "Stefan blowing, Navier slip, and radiation effects on thermo-solutal convection from a spinning cone in an anisotropic porous medium," *Journal of Porous Media*, vol. 19, no. 7, pp. 617–633, 2016.
- [37] Amirson, N., Uddin, M. J., and Ismail, A. I. M., "Electromagnetoconvective stagnation point flow of bionanofluid with melting heat transfer and Stefan blowing," *Thermal Science*, vol. 22, pp. 134-134, 2017.
- [38] Basir, M. F. M., Uddin, M. J., Bég, O. A., and Ismail, A. M., "Influence of Stefan blowing on nanofluid flow submerged in microorganisms with leading edge accretion or ablation," *Journal of the Brazilian Society of Mechanical Sciences and Engineering*, vol. 39, no. 11, pp. 4519-4532, 2017.
- [39] Giri, S. S., Das, K., and Kundu, P. K., "Stefan blowing effects on MHD bioconvection flow of a nanofluid in the presence of gyrotactic microorganisms with active and passive nanoparticles flux," *The European Physics Journal Plus*, vol. 132, no. 101, 2017.
- [40] Zohra, F. T., Uddin, M. J., Ismail, A. I. M., Bég, O. A., and Kadir, A., "Anisotropic slip magneto-bioconvection flow from a rotating cone to a nanofluid with Stefan blowing effects," *Chinese Journal of Physics*, vol. 56, no. 1, pp. 432-448, 2018.

- [41] Amirson, N. A., Uddin, M. J., Izani, A., and Ismail, M., "MHD boundary layer bionanoconvective non-Newtonian flow past a needle with Stefan blowing," *Heat Transfer*, vol. 48, no. 2, pp. 727-743, 2019.
- [42] Martini, A.; Hsu, H.; Patankar, N.A.; Lichter, S. Slip at high shear rates. *Phys. Rev. Lett.* 100, 2060011–2060014, 2008.
- [43] Liu, Y.; Gehde, M. Effects of surface roughness and processing parameters on heat transfer coefficient between polymer and cavity wall during injection molding. *Int. J. Adv. Manuf. Technol.* 84, 1325–1333, 2016.
- [44] Y. Lou *et al.*, Wall slip behaviour of polymers based on molecular dynamics at the micro/nanoscale and its effect on interface thermal resistance, *Polymers* 2020, 12(10), 2182.
- [45] Nikolov A, Kondiparty K, Wasan D., Nanoparticle self-structuring in a nanofluid film spreading on a solid surface. *Langmuir Lett* 26:7665–7670 (2020).
- [46] Uddin, M. J., Béq, O. A., and Amin, N. S., "Hydromagnetic transport phenomena from a stretching or shrinking nonlinear nanomaterial sheet with Navier slip and convective heating: a model for bio-nano-materials processing," *Journal of Magnetism and Magnetic Materials*, vol. 368, pp. 252–261, 2014.
- [47] Uddin, M. J., Khan, W. A., and Amin, N. S., "G-Jitter mixed convective slip flow of nanofluid past a permeable stretching sheet embedded in a Darcian porous media with variable viscosity," *PLoS One*, vol. 9, no. 6, pp. e99384, 2014.
- [48] Uddin, M. J., Ferdows, M., and Béq, O. A., "Group analysis and numerical computation of magneto-convective non-Newtonian nanofluid slip flow from a permeable stretching sheet," *Applied Nanoscience*, vol. 4, no. 7, pp. 897–910, 2014.
- [49] Uddin, M. J., Khan, W. A., Ismail, A. I. M., "Melting and second order slip effect on convective flow of nanofluid past a radiating stretching/shrinking sheet," *Propulsion and Power Research*, vol. 7, no. 1, pp. 60-71, 2018.
- [50] Mishra, U., and Singh, G., "Dual solutions of mixed convection flow with momentum and thermal slip flow over a permeable shrinking cylinder," *Computers and Fluids*, vol. 93, pp. 107–115, 2014.
- [51] Kishore, N., and Ramteke, R. R., "Slip in flows of power-law liquids past smooth spherical particles," *Acta Mechanica*, vol. 226, no. 8, pp. 2555-2571, 2015.
- [52] Shateyi, S., and Mabood, F., "MHD mixed convection slip flow near a stagnation-point on a nonlinearly vertical stretching sheet in the presence of viscous dissipation," *Thermal Science*, vol. 21, no. 6B, pp. 219-219, 2015.
- [53] Khan, W. A., Uddin, M. J., and Ismail, A. I. M., "Multiple slip effects on unsteady MHD rear stagnation point flow of nanofluids in a Darcian porous medium," *Journal of Porous Media*, vol. 18, pp. 665–678, 2015.

- [54] Basir, M. F. M., Uddin, M. J., Ismail, A. M., and Bég, O. A., "Nanofluid slip flow over a stretching cylinder with Schmidt and Péclet number effects," *American Institute of Physics Advances*, vol. 6, no. 5, pp. 055316, 2016.
- [55] Rosca, N. C., Rosca, A. V., Aly, E. H., and Pop, I., "Semi-analytical solution for the flow of a nanofluid over a permeable stretching/shrinking sheet with velocity slip using Buongiorno's mathematical model," *European Journal of Mechanics B Fluids*, vol. 58, pp. 39-49, 2016.
- [56] Uddin, M. J., Alginahi, Y., Bég, O. A., and Kabir, M. N., "Numerical solutions for gyrotactic bioconvection in nanofluid-saturated porous media with Stefan blowing and multiple slip effects," *Computers and Mathematics with Applications*, vol. 72, no. 10, pp. 2562-2581, 2016.
- [57] MD. Shamshuddin, M. Ferdows, O. Anwar Bég, Tasveer A. Bég and H. J. Leonard, Computation of reactive thermosolutal micropolar nanofluid Sakiadis convection flow with gold/silver metallic nanoparticles, *Waves in Random and Complex Media* (2022). <https://doi.org/10.1080/17455030.2022.2051773> (37 pages)
- [58] M. Ferdows, Tahia Tazin, K. Zaimi, O. Anwar Bég and T.A. Bég, Dual solutions in Hiemenz flow of an electro-conductive viscous nanofluid containing elliptic single-/multi-wall carbon nanotubes with magnetic induction effects, *ASME Open Journal of Engineering*, 1, 011040-1 to 011040-14 (2022).
- [59] M. Saleem, M. Hussain and M. Inc, Significance of Darcy–Forchheimer law and magnetic field on the comparison of Williamson–Casson fluid subject to an exponential stretching sheet, *International Journal of Modern Physics B*, Vol. 37, No. 27, 2350315 (2023).
- [60] M. Saleem, M. Hussain, Dual solutions of Williamson-Casson fluid over a heated exponentially shrinking surface with stability analysis: A novel Cattaneo-Christov heat flux model combination, *Numerical Heat Transfer, Part A: Applications*, *An International Journal of Computation and Methodology*, 85, 114-136 (2024).